Perturbations of a Planet on the β Pictoris Circumstellar Dust Disk

3. Time Scale of Collisional Destruction versus Resonance Time Scale

A. Lecavelier des Etangs

Institut d'Astrophysique de Paris, 98bis Bld Arago, F-75014 Paris, France
E-mail: lecaveli@iap.fr

H. Scholl

Observatoire de Nice-Cote d'Azur, Le Mont-Gros, F-06000 Nice, France

F. Roques and B. Sicardy

Observatoire de Meudon, DESPA, F-92195 Meudon Cedex, France

and

A. Vidal-Madjar

Institut d'Astrophysique de Paris, 98bis Bld Arago, F-75014 Paris, France

We have already shown that a planet orbiting β Pictoris is able to confine the circumstellar dust. Here we present new numerical simulations which improve this model. The new model takes into account destructive collisions between particles, and looks at the steady state between the collision and the dust replenishment. We show that there exists a critical value of the normal optical depth ($\tau_{\mathrm{op_c}} \sim 4 \times 10^{-4}$) and if the optical depth is smaller than this critical value in the resonant region (20–50 AU), asymmetric structures are created by the planet and maintained in spite of collisions. Although these structures cannot explain the asymmetries now observed in the disk, they could be a way to reveal bodies otherwise invisible by direct imagery. © 1996 Academic Press, Inc.

1. INTRODUCTION

In previous papers, we have already discussed the effect of a planet embedded in a circumstellar dust disk (Scholl *et al.* 1993, Roques *et al.* 1994, Lazzaro *et al.* 1994). In particular, we have investigated numerically and analytically the possibility of dust confinement by a planet orbiting β Pictoris. Above a critical planet mass of $\approx 10^{-5}$ stellar mass (5 Earth masses), the particles are trapped in outer mean motion resonances. Although not permanent, this trapping can create a steady state clearing zone extending

inside the planet orbit, which could explain the depletion region recently observed with 10 μm imagery (Lagage and Pantin 1994).

However, comparing the different time scales of evolution in the β Pictoris disk, Backman and Paresce (1993) conclude on two very important points: the grain lifetimes are shorter than the stellar age, thus the disk must be continually replenished, and the Poynting–Robertson (PR) time scale is comparable to the collision time scale. Moreover, the collisions can be assumed to result in destruction rather than in accretion, because collisions at relative speed larger than 0.5 km sec^{-1} should result in catastrophic fragmentation, the fragments being small enough to be quickly ejected from the disk trough radiation pressure.

In the preceding papers, we have shown that asymmetric structures, like accumulation of matter or arc-like structures can be created by particles which are brought by PR drag into mean motion resonances with a hypothetical planet. Theses structures could be directly observed and give indirect evidence of the presence of a planet. Asymmetries have already been observed in the β Pictoris disk (Lecavelier des Etangs *et al.* 1993, Golimowski *et al.* 1993, Lagage and Pantin 1994, Kallas and Jewitt 1995), and the light variation of the star could be compatible with such structure passing in front of β Pictoris (Lecavelier des

Etangs *et al.* 1995). However, the problem of the different time scales raises the question whether these structures can survive the collisional destruction. If they effectively survive, we have to ask if they can be the origin of the asymmetries now observed in the disk.

In order to investigate these questions and with the normal optical depth given by observation ($\tau_{op} \sim 2 \times 10^{-4}$, Backman *et al.* 1992, Lagage and Pantin 1994), we have carried out new numerical and few analytical calculations in order to compare these time scales and evaluate the consequences for the β Pictoris disk. The model is presented in Section 2. Then, we discuss the comparison of the different time scales in Section 3. Finally, the results and the discussion are given in Sections 4 and 5.

2. THE MODEL

2.1. General Layout

We have already studied in details the consequences of the mass of the planet (Roques *et al.* 1994, Lazzaro *et al.* 1994), concluding that there exists a critical planet mass of $10^{-5}\, M_\star$, i.e. about 5 Earth masses, or 1/3 uranian masses, above which trapping in mean motion resonances is very efficient. In this paper, we have only considered an unique planet mass of $10^{-4}\, M_\star$ with a semi-major axis of $a_0 = 20$ AU. For β Pictoris, the stellar mass is $M_\star = 1.5\, M_\odot$.

We have integrated the complete motion of particles under the gravitational field of the star and the planet, the radiation pressure, and the PR drag (Burns *et al.* 1979). The integration has been carried out by a Bulirsh–Stoer integrator implemented on a CM5 Connection Machine, a massively parallel computer.

Unlike the previous models, we assume a size distribution for the particles and thus also for the dissipative coefficient, β, which is the ratio of the radiation force to the gravitational force of the star. Indeed, for particles with radius $s \geq 1\ \mu m$, β is correlated to the sizes of the particle by $\beta \propto s^{-1}$ (Artymowicz 1988). The origin of particles is not known but the disk is supposed to be replenished either by colliding or evaporating kilometer-sized bodies. We can assume a size distribution in power law like in comet dust (Lien 1990 and reference therein), in collisionally replenished dust (Greenberg and Nolan 1989), or in the interplanetary medium (Le Sergeant d'Hendecourt and Lamy 1980). Thus, if we have a size distribution $dn \propto s^p ds$, then we have $dn \propto \beta^q d\beta$ with $q = -p - 2$. Here we consider the classical $p = -3.5$ (collisional sources) that is $q = 1.5$.

We have roughly $\beta \sim (s/1\ \mu m)^{-1}$, but since only β is important in simulations, the exact relation between β and s is not necessary and even depends on dust composition. We have taken $\beta \in [0.1, 0.4]$, $W = \beta_{min}/\beta_{max} = 4$ is thus quite small. But particles with small β are large particles, less numerous, and very quickly destroyed by collisions.

They do not change the result of the runs: test runs have been done, for example run Ia (See Section 4) with $\beta \in [0.0, 0.4]$ ($W \to \infty$) and the results were the same.

2.2. Collisions

The relative velocities in collisions highly depends on the relative inclination and eccentricities of the trajectories. With on opening angle of about 8° (Artymowicz 1989), at a distance less than 30 AU from the star, the relative motion velocity is larger than 0.5 km sec^{-1}. Thus the collision should result in catastrophic fragmentation (Backman and Paresce 1993, Lissauer and Griffith 1989 and references therein), each fragment being quickly blown-out by the radiation pressure. Thus, when in the runs a particle is supposed to have a collision, it is simply eliminated from the simulation.

Since the particles are continuously eliminated by collisions, and the disks exist and last much longer than the collision time, they must be replenished (Backman and Paresce 1993). The explanation of the dust origin is outside the scope of this paper. We have only added particles during the run with a constant injection rate and orbital parameter distribution similar to the initial conditions (Section 2.3). After a relaxation time (about 6000 revolutions), the system goes into a steady state. This steady state will last as long as the disk is replenished and is considered as the result of the run.

2.3. Initial Condition

We have chosen to begin with 2000 particles and we have selected the parameters in order to have about 5000 particles at the steady state stage. The initial conditions are defined by the orbit parameters of the planet and the particles. The planet is at a radius of 20 AU with an eccentricity of either 0 or 0.01. The particles have an inclination between 0° and 8°. We have chosen to begin with particles on circular orbit ($e = 0$). If the initial eccentricities of particles were smaller than 0.05, the particles would also be trapped in resonance (Lazzaro *et al.* 1994) and the observed structures in Figs. 3 to 7 would not be changed. However for larger eccentricities, the particles are not trapped. The particle initial positions and their angle of the node are randomly distributed between 0° and 360°. The different initial conditions are summarized in Table I and can be seen in Figs. 3 to 7.

2.4. Physical Parameters

2.4.1. Numerical model for the collisions. As the collisions destroy the particles, it is not important to model them exactly. Only the percentage of destructed particles is important, thus we will estimate a probability of collision for each particle as a function of the particle density and the velocity relative to the neighbor particles. If P_i is the

TABLE I
The Five Runs and the Results

	Input				Output		
Run	e_{planet}	$a_{\mathrm{particles}}$ (AU)	$\overline{\sigma}$ (AU^2)	I (part. T_0^{-1})	N	τ_{op}	Result
Ia	0	[30; 32]	5×10^{-5}	3.2	3770	1.4×10^{-4}	$t_{\mathrm{res}}/t_{\mathrm{coll}} = 8.4$ resonance 2:1, structures at 260° from the planet
Ib	0.01						
IIa	0	[24; 32]	5×10^{-5}	3.2	4150	1.6×10^{-4}	$t_{\mathrm{res}}/t_{\mathrm{coll}} = 9.6$ resonance 2:1 and 3:2, structures at 270° and 100° from the planet
IIb	0.01						
III	0	[24; 32]	2.5×10^{-4}	16	4715	9×10^{-4}	too few particles in resonance

probability that the particle i of size s_i is collisionally elimi-nated during the time dt by a collision with one of the $j \neq i$ particle with a size s_j in the volume V containing n particles, then

$$P_i = \sum_{j \neq i}^{n} \frac{\|\mathbf{v}_j - \mathbf{v}_i\| \, \pi(s_j + s_i)^2 \, dt}{V}. \quad (1)$$

For the numerical simulation we have assumed that $\|\mathbf{v}_j - \mathbf{v}_i\| \approx \|\overline{\mathbf{v}} - \mathbf{v}_i\|$, where $\overline{\mathbf{v}} = \sum_{j=1}^{n} \mathbf{v}_j/n$ and $\pi(s_j + s_i)^2 \approx \pi \overline{s}^2(1 + s_i/\overline{s})^2$, where $\pi \overline{s}^2 = \overline{\sigma}$ is the mean cross section of the particles, and is a parameter of the model. Moreover, we have $s_i/\overline{s} = (\beta_i \cdot \overline{1/\beta})^{-1}$, where $\overline{1/\beta}$ is the mean value of β^{-1}.

We divide the three dimensional space in a mesh of cells. We computed P_i for each particle i every dt (dt is between 1 and 4 times the period of the planet) in the surrounding cell of volume V. Thus, if the particle i is in a cell containing n particles, every time step dt we eliminate this particle with a probability.

$$P_i = \frac{n}{V} \|\overline{\mathbf{v}} - \mathbf{v}_i\| \overline{\sigma}(1 + s_i/\overline{s})^2 \, dt. \quad (2)$$

The probability P_i for the particle i to have a collision is proportional to the difference between the particle velocity and the mean velocity in the cell. It also depends on the particle density in the cell.

The choice of the size of the cells has been made in order to minimize the mean of the differences of the mean velocities computed in adjacent cells. As can be seen in Fig. 1, the optimal size of the cells is around 1.3 AU. We used a mesh of $48 * 48 * 6$ cells over $64 * 64 * 8$ AU^3, which corresponds to cells with a size of 1.33 AU.

The statistical treatment of the collisions has been com-pared to "true collision" simulations. These last ones are very time consuming, and have been carried out on a steady

state similar to the result of the run Ia, but with only 700 particles. For example, after 13 revolutions of the planet, 5 "true collisions" have destroyed 10 particles, which must be compared to the mean of 8.3 particles destroyed per 13 revolutions in the statistical treatment. Other tests have been performed; it has been found that generally Eq. (2) gives an underestimate of about 20–25% in the collision
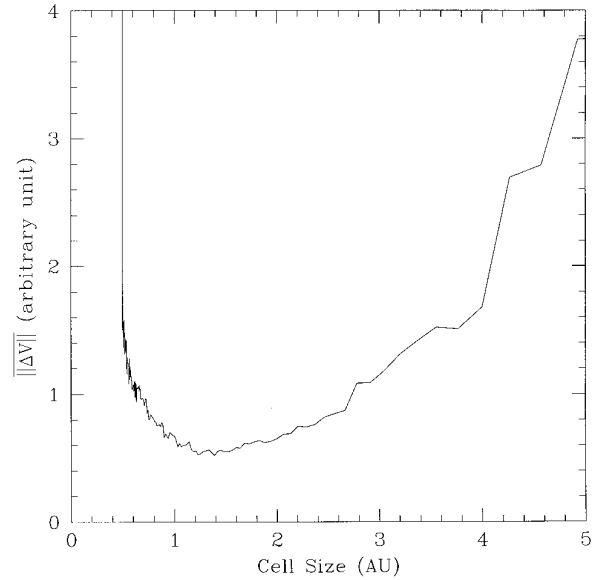

FIG. 1. Plot of the mean of the differences of mean velocities between neighbor cells as a function of the cell size. If the cells are too large, the distance between the particles of the two cells is large and their velocities are significantly different. That means that the mean velocity of the cell **v** is significantly different from the velocity which is expected to represent the flux of other particles where the particle i is located. In contrast, if the cells are too small, the number of particles in the cell are too small and the peculiar motion of the particles can disturb the mean velocity estimation. This calculation has been carried out after 2000 revolutions with the same initial conditions as in run Ia. The optimal size of the cells is about 1.32 AU.

rate. Thus, although the collisions are evaluated only statistically, all conclusions given here are validated. Moreover, it is noteworthy that the numerical method carries complete information of the particle orbits.

2.4.2. Connection between numerical and physical parameter. We have now to decide the value of the parameters in the model, and to evaluate the connection between these parameters and the real ones of the circumstellar disk. The input parameters are essentially $\overline{\sigma}$ and I, the injection rate of particles during the run. We have taken I constant. Finally, the most important physical parameter which connects the N particles in the run to the real dust is τ_{op}, the normal optical depth of the disk. How must we choose I and $\overline{\sigma}$ in order to achieve a τ_{op} given by the observation, and N compatible with the available CPU time?

If the N particles are spread over an area S, because we consider optical depth small with respect to 1, we have

$$\tau_{\mathrm{op}} = \frac{\sum_{i=1}^{N} \pi s_i^2}{S} = \frac{N\pi\overline{s}^2 \int (s_i/\overline{s})^2 \, dn_i}{S \int dn_i}. \tag{3}$$

We obtain

$$\tau_{\mathrm{op}} = \frac{N\overline{\sigma}\lambda}{S}, \tag{4}$$

where

$$\lambda = \frac{\int (s_i/s)^2 \, dn_i}{\int dn_i} = \frac{\int \beta^{-2} \, dn}{(\overline{1/\beta})^2 \int dn}. \tag{5}$$

If $\beta \in [0.1, 0.4]$ and with $q = 1.5$, $W = 4$ and $\lambda = 1.14$. For $W \to \infty$, $\lambda \to 1.8$.

Moreover, if we assume that each orbiting grain encounters the full surface density twice per orbit, the mutual collision time scale is

$$t_{\mathrm{coll}_i} = \frac{T_i}{2 \sum_{j=1}^{N} (\pi(s_i + s_j)^2/S)}, \tag{6}$$

T_i being the revolution period of the particle i. From the equations given in Section 2.4.1, we have

$$t_{\mathrm{coll}_i} = \frac{T_i S}{2N\overline{\sigma}(1 + 1/(\beta_i \cdot \overline{\beta^{-1}}))^2}. \tag{7}$$

That is

$$t_{\mathrm{coll}_i} = \frac{T_i \lambda}{2\tau_{\mathrm{op}}(1 + 1/(\beta_i \cdot \overline{\beta^{-1}}))^2}. \tag{8}$$

In particular, if there is a unique value of β, that is single sized particles, then

$$\begin{cases} \lambda = 1 \\ (1 + 1/(\beta_i \cdot \overline{\beta^{-1}}))^2 = 4 \end{cases} \tag{9}$$

$$t_{\mathrm{coll}} = \frac{T}{8\tau_{\mathrm{op}}}. \tag{10}$$

We obtain the classical formula as a special case where there is no size distribution.

We have

$$\frac{I \, dn}{\int dn} = \frac{N \, dn_{\mathrm{s}}}{t_{\mathrm{coll}}(\beta) \int dn_{\mathrm{s}}}, \tag{11}$$

where $dn \propto \beta^q \, d\beta$ is the size distribution of the injected particles and dn_{s} is the size distribution of the particle at the steady state, then

$$dn_{\mathrm{s}} \propto \frac{\beta^q \, d\beta}{(1 + (1/\beta \cdot \overline{\beta^{-1}}))^2}. \tag{12}$$

As we will see in Section 4.3, this distribution is effectively observed at the steady state in the runs.

And from Eqs. (7) and (11),

$$I = \frac{2N^2\overline{\sigma}\mu}{T_i S}, \tag{13}$$

where

$$\mu = \frac{\int \beta^q \, d\beta}{\int \beta^q \, d\beta/(1 + (1/\beta \cdot \overline{\beta^{-1}}))^2}. \tag{14}$$

$\mu = 3.7$ for $W = 4$, and $\mu \to 3.5$ if $W \to \infty$.

Let us now assume that the particle i is in mean motion resonance $j{:}j + 1$ with the planet of period T_0. Then $j \cdot T_i = (j + 1) \cdot T_0$. From Eqs. (4) and (13), we obtain the equations which define the input parameters:

$$\begin{cases} \overline{\sigma} = \frac{\tau_{\mathrm{op}} S}{N\lambda} \\ I = \frac{2\tau_{\mathrm{op}} N\mu}{\lambda T_0} \frac{j}{j + 1}. \end{cases} \tag{15}$$

2.5. Keplerian Bias

In fact, the relative Keplerian motion of the particles in the same cell causes a slight increase ΔP of the probability of elimination, with no physical signification.

$$\Delta P \cong 4 \frac{n}{V} \|\Delta\mathbf{v}\| \overline{\sigma} \, dt, \tag{16}$$

where $\Delta\mathbf{v}$ is the relative Keplerian velocity inside the cell.

$$\|\Delta\mathbf{v}\| \leq \frac{\|\mathbf{v}\|(l/2)}{2d_{c\star}} = \frac{\pi l}{2T_i}, \tag{17}$$

where l is the size of the cell and $d_{c\star}$ the distance between the cell and the star. Since $n/V = N/Sh$, if h and S are the height and the area of the system, and $NP = I \, dt$, we have

$$\frac{\Delta P}{P} \cong \frac{2\pi N^2 l \overline{\sigma}}{ShIT_i} = \frac{\pi l}{\mu h}. \tag{18}$$

With the parameters of the models and the chosen size of the cells ($l = 1.33$ AU, $h = 8$ AU), we have $\Delta P/P \cong 0.14$.

3. TIME SCALES: MEAN MOTION RESONANCES VERSUS COLLISIONS

Following Weidenschilling and Jackson (1993), for a particle which has entered in mean motion at $t = 0$ with an initial eccentricity $e_0 = 0$,

$$e(t) = e_{max}\sqrt{1 - e^{-t/t_{res}}} \tag{19}$$

with

$$e_{max} = \sqrt{\frac{2}{5j - 1}} \tag{20}$$

and

$$t_{res} = \frac{a_0^2 c}{GM_\star} \frac{(1 - \beta)^{2/3}}{\beta} \left(\frac{j + 1}{j}\right)^{4/3} \left(\frac{j + 1}{5j - 1}\right). \tag{21}$$

If we take the collisions into account, at the steady state and assuming a constant injection rate of particles, for a given e in the eccentricity space, there is an equilibrium between input from smaller eccentricities by resonances and output through collisional destruction. Then $n(e)$ the distribution of the eccentricities follows the law

$$n(e) \, de \propto \frac{e^{-t/t_{coll}}}{(de/dt)_e} \, de. \tag{22}$$

From Eq. (19), we conclude that

$$n(e) \, de \propto e(e_{max}^2 - e^2)^{t_{res}/t_{coll}-1} de. \tag{23}$$

As we will see in Section 4.4, this law is a very good approximation of the distribution of the eccentricities observed in the runs.

To obtain the density structures supplied by mean motion resonances, dust grains must have enough time to increase their eccentricities before being destroyed by collisions. Thus, density structures exist providing that large eccentricities are populated enough. Then, the critical parameter which is related to the existence and strength of the density structures in the disk is the ratio t_{res}/t_{coll}. Indeed, if $t_{res} > t_{coll}$, the maximum of $n(e)$ is obtained with $e = e_0 = e_{max}/(\sqrt{2t_{res}/t_{coll} - 1})$, and structures are visible if $e_0 \gtrsim 0.1$, that is $t_{res}/t_{coll} \leq 25$. We have

$$\frac{t_{res}}{t_{coll}} = \frac{2a_0^2 c\tau_{op}}{T_0 \lambda GM_\star} \frac{(1 - \beta)^{2/3}}{\beta} \cdot (1 + (\beta\overline{\beta^{-1}})^{-1})^2$$
$$\cdot \left(\frac{j + 1}{j}\right)^{1/3} \left(\frac{j + 1}{5j - 1}\right). \tag{24}$$

Thus

$$\frac{t_{res}}{t_{coll}} = \frac{c\tau_{op}}{\pi\lambda} \left(\frac{a_0}{GM_\star}\right)^{1/2} \cdot f(\beta) \cdot g(j), \tag{25}$$

where f and g contain the β and j dependence of Eq. (24). In the case of β Pictoris ($M_\star = 1.5 \, M_\odot$),

$$\frac{t_{res}}{t_{coll}} = 1.17 \cdot 10^4 \frac{\tau_{op}}{\lambda} \left(\frac{a_0}{20 \, \text{AU}}\right)^{1/2} f(\beta)g(j). \tag{26}$$
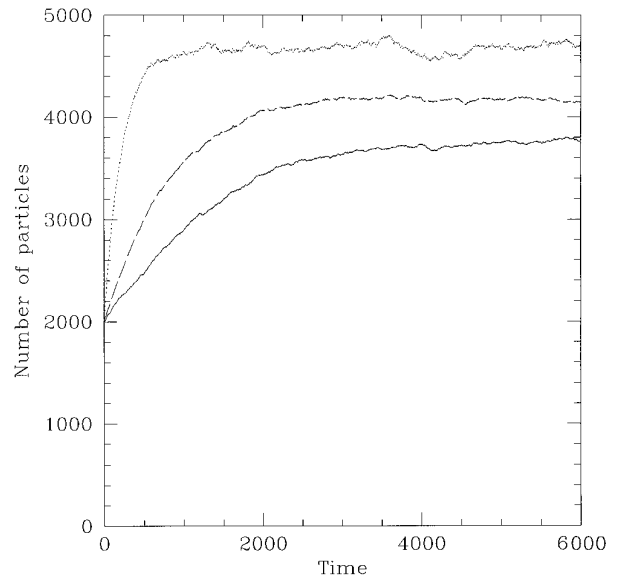
FIG. 2. Plot of the number of particles during the runs. The steady states are obtained after about 6000 revolutions. Runs I, solid line; Runs II, dashed line; Run III, dotted line.
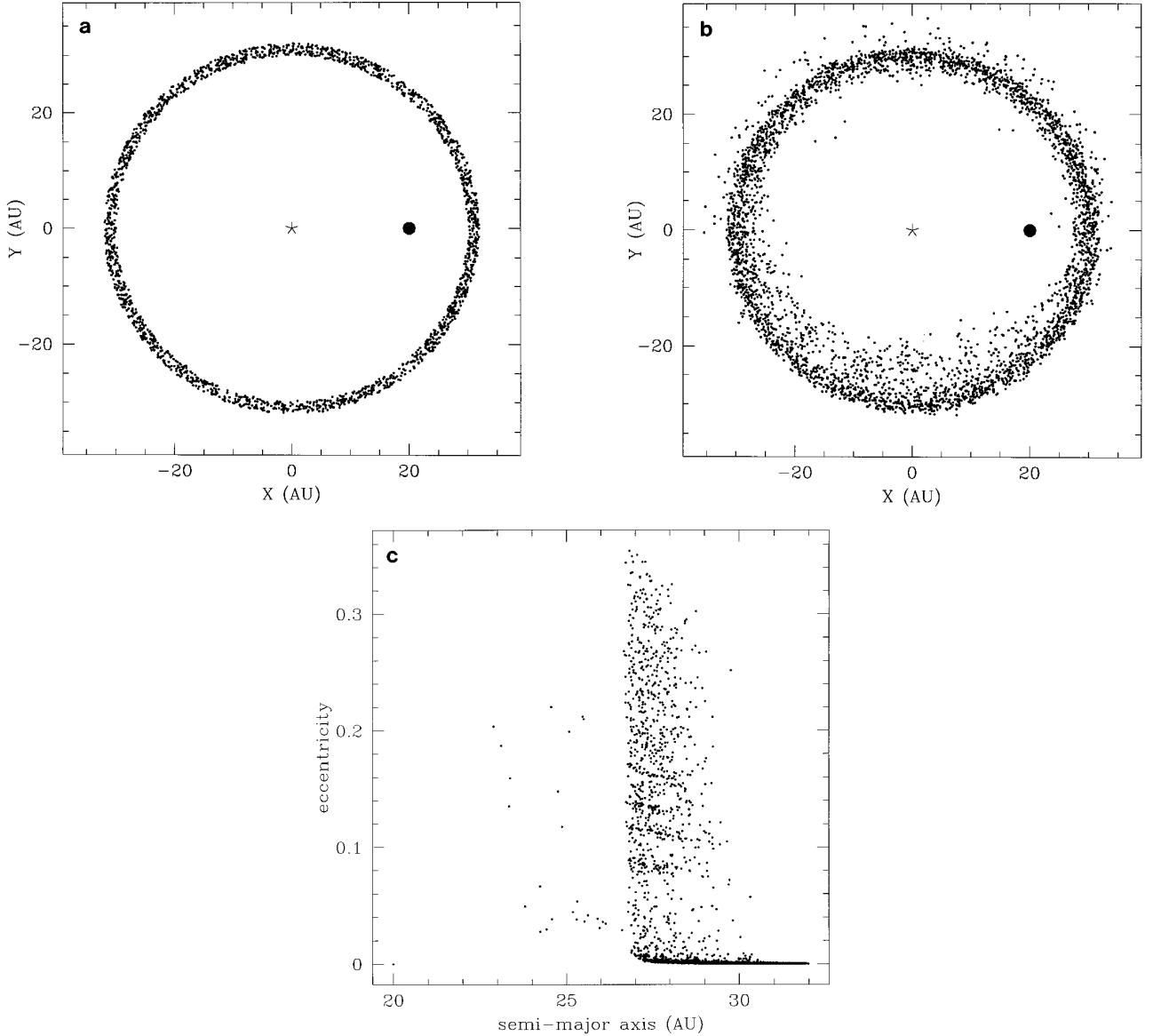
FIG. 3. Plot of run Ia. (a) The initial distribution of the particles. The planet is represented by a black dot and β Pictoris by a star. (b) The spatial distribution after 6000 revolutions (4×10^5 years). There is an accumulation of matter at the bottom of the figure around 270° from the planet. (c) Positions of the particles in the a–e diagram (eccentricity versus semi-major axis). Very few particles can escape from the 2:1 resonance, and then they are trapped in 3:2 resonance. Due to the different sensitivity to the radiation pressure (β coefficient), the locations of the resonances are spread over several AU.

For $\beta = 0.3$, $f(\beta) \approx 10$ and with $j = 1$

$$\frac{t_{res}}{t_{coll}} = 6 \times 10^4 \left(\frac{a_0}{20\,\text{AU}}\right)^{1/2} \tau_{op}. \quad (27)$$

We conclude that there exists a critical τ_{op_c} for which $t_{res}/t_{coll} \leq 25$:

$$\tau_{op_c} = 4 \times 10^{-4} \left(\frac{a_0}{20\,\text{AU}}\right)^{1/2} \left(\frac{f(\beta)}{10}\right)^{-1}. \quad (28)$$

We will actually see that if t_{res}/t_{coll} is even greater than 10, since the eccentricity increases very quickly when the particles enter in mean motion resonance, the density structures can exist in the steady state resulting from collisions and replenishment.

4. RESULTS

4.1. Input Parameters

We have completed five runs with different initial conditions for the particles, the planet eccentricity, and the nor-
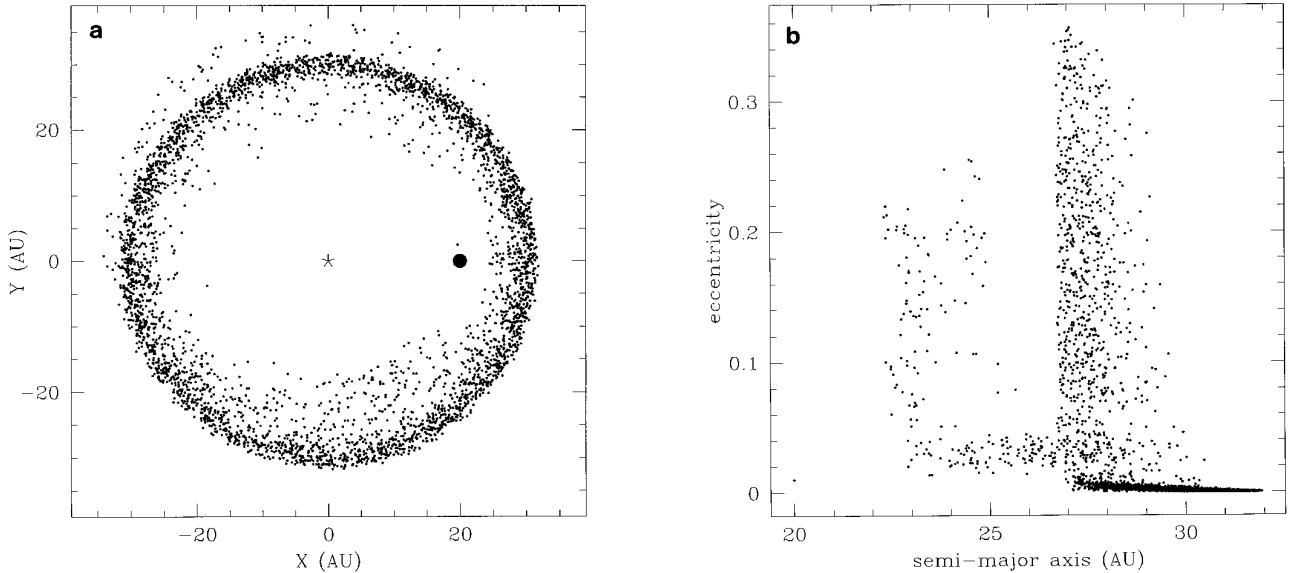
FIG. 4. Run Ib. (a) The spatial distribution after 6000 revolutions of planet with the same initial conditions as run Ia, except that here the planet has an eccentric orbit ($e = 0.01$). (b) We can see in the a–e diagram that few particles can escape the 2:1 and reach the 3:2 resonance.

mal optical depth. These conditions are summarized in Table 1. The input parameter $\bar{\sigma}$ has been calculated in order to have $\tau_{op} \sim 2 \times 10^{-4}$ in the first four runs (this corresponds to the value given by Backman *et al.* (1992) for the inside component of the β Pictoris disk, and the same value can be deduced from Lagage and Pantin (1994)), and $\tau_{op} \sim 10^{-3}$ in the last one, and also in order to have a steady state with about $N = 5000$ particles. We have only considered a planet with a mass of $10^{-4} \, M_\star$ and a semi-major axis of $a_0 = 20$ AU. As we can see in Table 1, although the statistical treatment of the collisions slightly underestimate the collision rate, the number of particles and normal optical depth are slightly smaller than the expected ones. This can be explained in part by the Keplerian bias in the cells (diminution of about 20% of the expected number of particles (Section 2.5)) and by the approximation in Eq. (6) from which input parameters have been carried out.

4.2. Steady State

In Fig. 2, we have plotted the number of particles in different runs as a function of time. It is obvious that after 6000 periods of the planet, the number of particles has reached an equilibrium. Moreover, there is no more evolution of the density distribution of the particles either in the (a, e) or in the (X, Y) plane. The steady state resulting from the destructive collisions and the replenishment has been reached.

We have plotted these steady states in Figs. 3 to 7 with the position of the particles after 6000 revolutions in the (X, Y) and the semi-major axis versus eccentricity (a, e)

planes. The over-densities are easily seen in the first diagram, and we can see that most of the particles are trapped in mean motion resonance with the planet. In the first run, all the particles which cross the 2:1 resonance semi-major axis effectively enter this resonance. In the run II, some particles have initial conditions with a semi-major axis smaller than the semi-major axis of 2:1 resonance, thus their semi-major axis decreases down to the 3:2 resonance. We see that the location of resonances is spread over a few AU; this is simply due to the fact that the particles have a size distribution, and that the critical semi-major axis depends on the β parameter and decreases as β increases (see Weidenschilling and Jackson 1993, for example). The ratio of the maximum semi-major axis to the minimum semi-major axis in resonance is $a_{max}/a_{min} = ((1 - \beta_{min})/(1 - \beta_{max}))^{1/3} = 1.14$.

4.3. Particle Size Distribution

We have plotted in Fig. 8 the particle size distribution (i) of the injected particles and (ii) of the particles at the steady state. It can be seen that large particles are very effectively destroyed. The distribution observed at the steady state is very similar to that predicted by Eq. (12). Morevoer, the β-dependence of the ratio t_{res}/t_{coll} (dashed line in Fig. 8) contributes to the fact that structures are observed and mainly due to the smallest particles.

4.4. Eccentricity Distribution

As already stated in Section 3, density structures can exist provided that large eccentricities are populated enough. To confirm the surprising result that density struc-
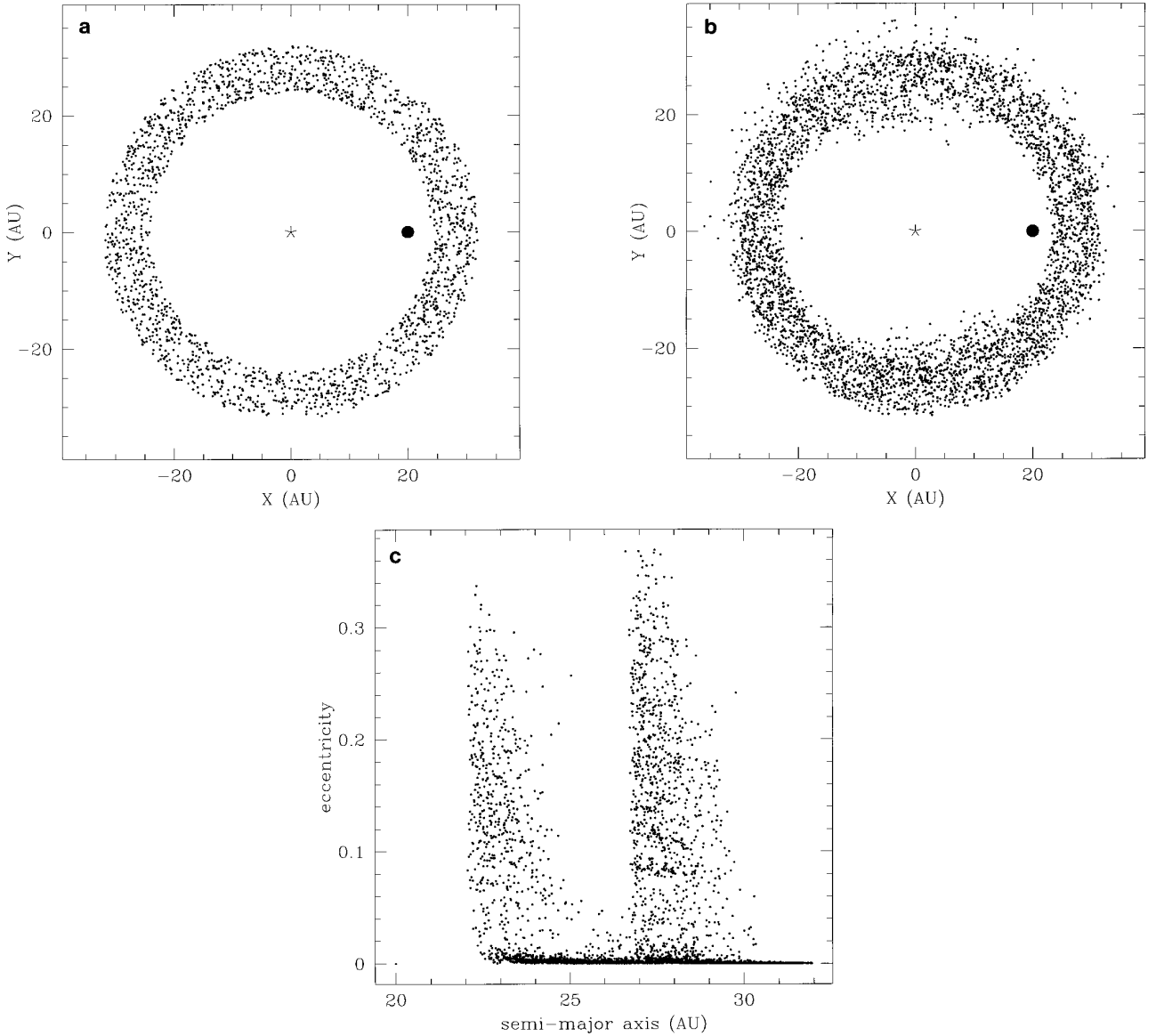
FIG. 5. Run IIa. (a) Plot of the initial conditions. Here the initial semi-major axis of the particles lies between 24 and 32 AU. (b) Plot of the steady state after 6000 revolutions of planet. (c) *a–e* diagram. Since the initial semi-major axis of some particles are smaller than the semi-major axis of the 2:1 resonance, they decay until they reach the 3:2 resonance. Thus, at the steady state, the particles are either in 2:1 or in 3:2 resonances.

tures still exist in the first four runs, although the collision time (t_{coll}) is about ten times smaller than the resonance time scale (t_{res}), we have plotted the density distribution of the eccentricities (Fig. 9). We find that this distribution follows that predicted (Eq. 23). Thus, we can conclude that the effect of the planetary resonances could be visible even if $t_{res} > t_{coll}$.

4.5. Spatial Distribution of the Collisions

The azimuthal distribution of collisions in the run IIb has been plotted in Fig. 10. It is obvious that this distribution relative to the planet position is not uniform, and presents a maximum at about 100° and a minimum around 250°. In this case, collisions are mainly due to particles which are in two different resonances. In order to explain this phenomenon, we have evaluated the relative velocity of two particles which are assumed to be in the strongest 2:1 resonance for the first particle ($j = 1$) and strongest 3:2 resonance for the second ($j = 2$). Then, we have

$$(j + 1)\theta_j - j\theta_0 - \omega = -\pi/2 \quad j = 1, 2, \qquad (29)$$

where $\theta_0 = 0$ is the longitude of the planet. We have a collision only if $\theta = \theta_1 = \theta_2$; for a given θ, we can evaluate
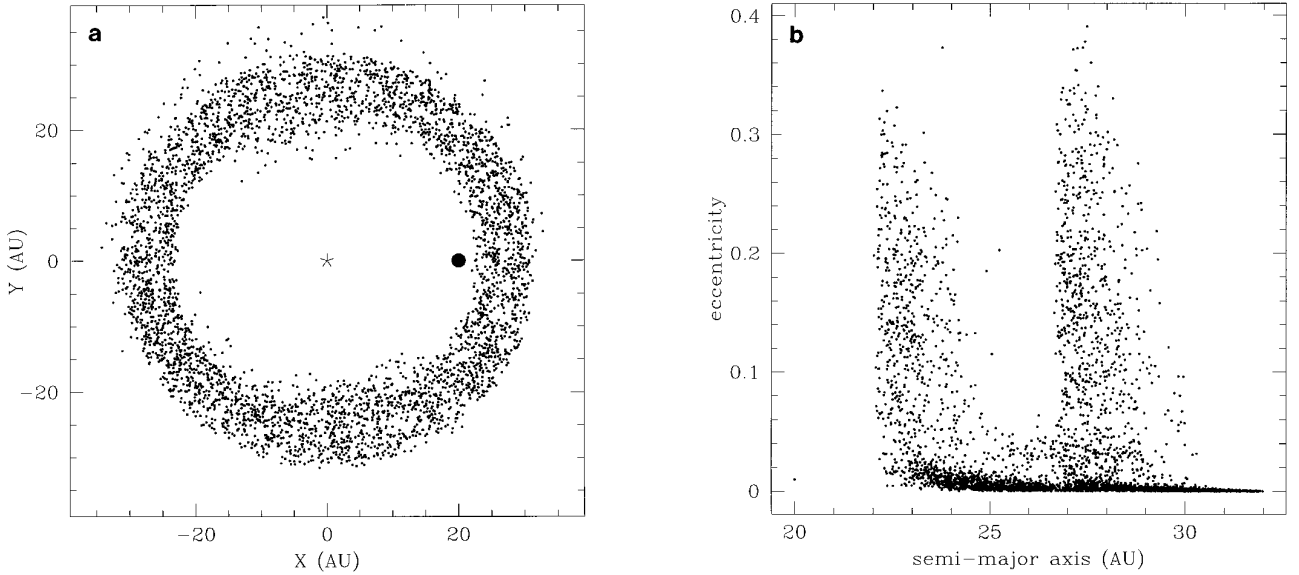
FIG. 6. Run IIb. (a) Same as run IIa with the planet in an eccentric orbit ($e = 0.01$). Here the steady state is very similar to the previous one. (b) a–e diagram.

V, the particle velocity as a function of E the eccentric anomaly which is calculated by solving Kepler's equation: $E_j - e_j \sin E_j = \theta_j - \omega_j = -\pi/2 - j\theta_j$. We have then plotted $\Delta V^2 = (\mathbf{V}_1 - \mathbf{V}_2)^2$ versus θ for $e_1 = 0.2$ and $e_2 = 0.1$ (Fig. 11). We see that the relative velocity of the particles in 2:1 and 3:2 mean motion resonances strongly depends on θ, as their mutual collisions. This very simple calculation is able to explain the maximum of the collision number around 120° from the planet, and the minimum between

220° and 280°. Thus, the production of small particles is not spatially uniform. The question of whether the parent bodies trapped in similar resonances can explain larger asymmetries (as proposed by Artymowicz 1995) is still open.

4.6. Radial and Azimuthal Distribution

Finally, the radial and azimuthal distribution of the particles is the quantity which can be observed with images
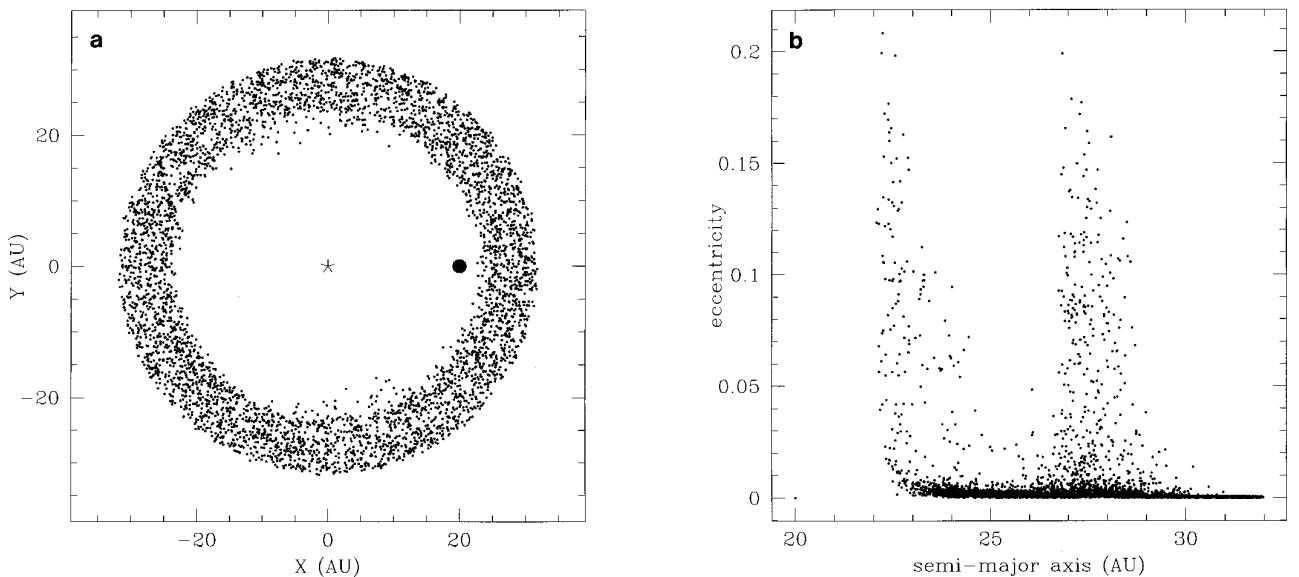

FIG. 7. Run III. (a) Plot of the steady state in run III with an optical depth of 9×10^{-4}. Here no structure can be observed. (b) We can see in the a–e diagram that some particles can be trapped in 2:1 and 3:2 resonances, but there are too many collisions and they do not spend a lot of time in these resonances. Thus, they do not increase their eccentricity enough to create asymmetric structures.
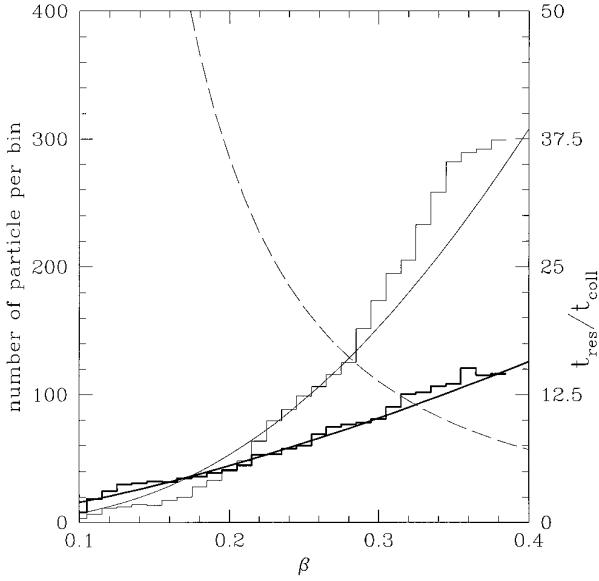
FIG. 8. Plot of the β distribution in run Ia (histogram) and the distribution predicted by Eq. (12) (solid line). Initial conditions, thick line. Steady state, thin line. It can be seen that large particles (small β) are more sensitive to collisional destruction that small particles. The dashed line shows the ratio t_{res}/t_{coll}. For $\beta \geq 0.25$, we see that $t_{res}/t_{coll} \leq 25$.
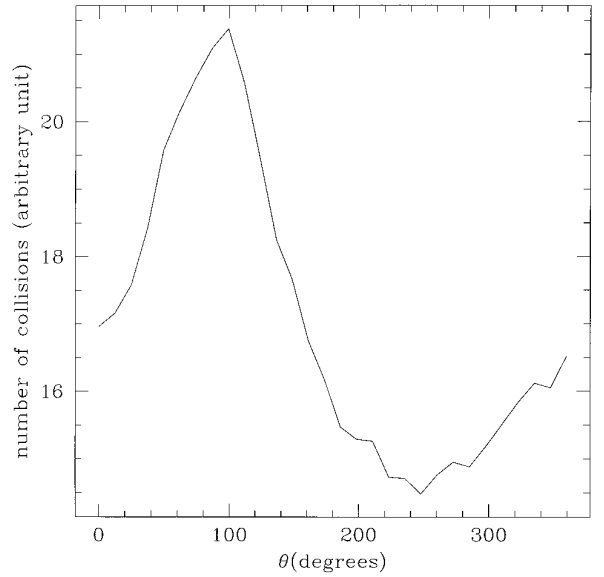

FIG. 10. Plot the collision distribution relative to the planet position observed in run IIb. The number of collisions reach a maximum around 100° and a minimum at about 250°. This figure is to be compared with Fig. 11.

or measurements of the variations of the star extinction through the dust disk. Figure 12 shows the radial distribution of dust for runs Ia and III. In the first case, radial distribution is not homogeneous and some features are visible. In Fig. 13, we have plotted $P(\theta)$, the probability that a particle has an angle between θ and $\theta + d\theta$, with

the planet. We see that an over-density of more than 10% is present in run I; the over-densities are 5% and 15% at 100° and 270° from the planet in run II. But, in run III, there is no observable feature since the normal optical
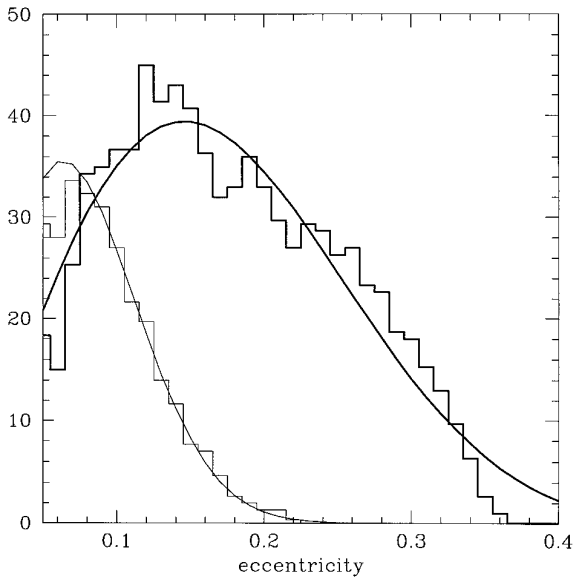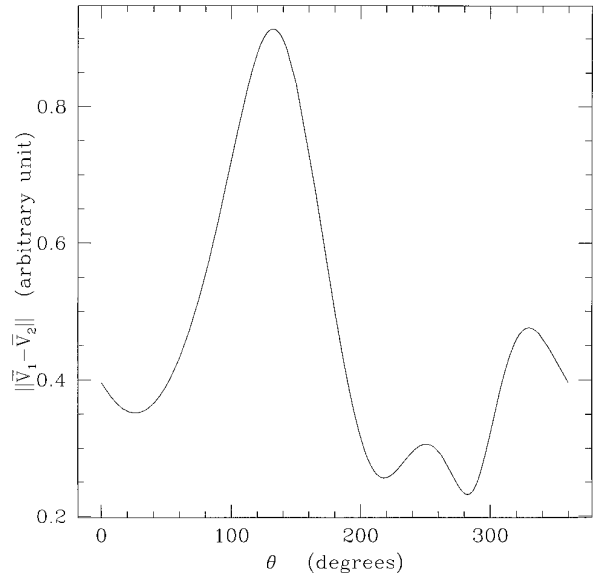

FIG. 9. Plot of the eccentricity distribution in runs (histogram) and the distribution predicted by Eq. (23) (solid line). Run I, thick line, Run III, thin line.

FIG. 11. The modulus of the relative velocity of two particles which are in the strongest resonance 2:1 and 3:2, versus θ, the longitude relative to the planet. The maximum is at 130° and the minimum between 220° and 280°. This shows that the spatial variations in the collision number density can be explained by collisions between particles in different mean notion resonances.
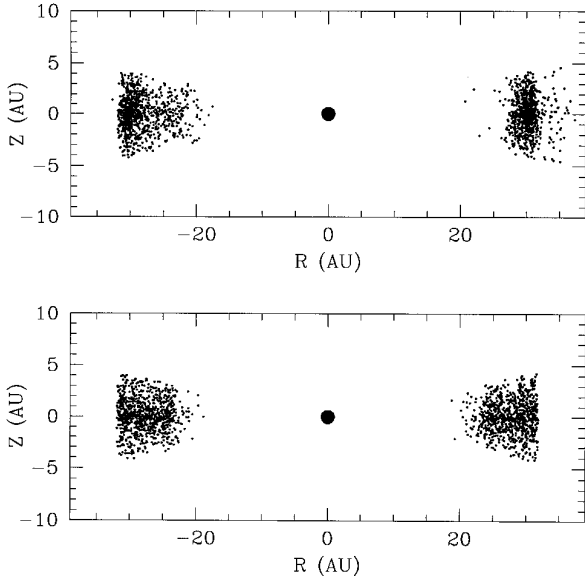
FIG. 12. Plot of the radial distribution of dust in runs Ia (upper) and III (lower). Only dust inside the quarters $|X| < |Y|$ has been represented with R having the same sign as Y. This image corresponds to the part of the disk seen edge-on from Earth if the line of sight is parallel to the X axis. For small optical depth (run Ia), a non-axisymmetrical radial extention of the dust could reveal the presence of a masssive body.

depth and the ratio t_{res}/t_{coll} are too large. Thus, the τ_{op} as measured by the most recent observations (Lagage and Pantin 1994) seems to be just under the value necessary to destroy the structures ($\tau_{op} \sim \tau_{op_c}/2$).
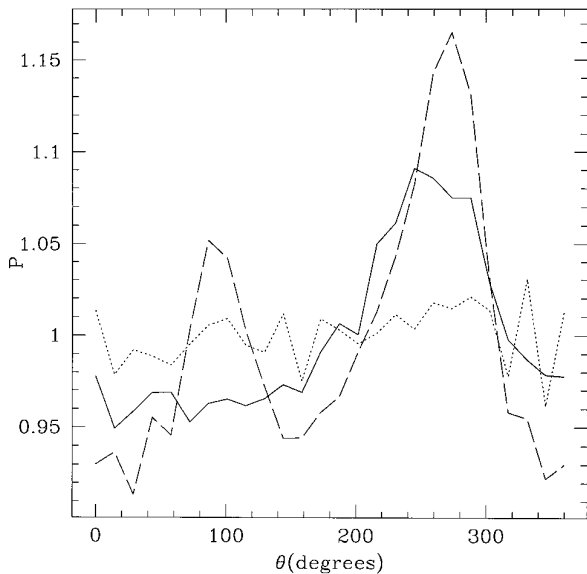

FIG. 13. The azimuthal distribution of particles in runs I (solid line), II (dashed line), and III (dotted line). We see that an over-density of more than 10% is present in the runs I; the over-densities are 5% and 15% at 100° and 270° from the planet in runs II. However, due to the larger normal optical depth, there is no observable characteristics in run III ($\tau_{op} = 9 \times 10^{-4}$).

5. DISCUSSION

The new model presented here is not only an analysis of physical processes (PR effect, resonances) which take place in disks. It is different from previous models not only because collisions are taken into account but also because of the assumed particle size distribution. Arc-like structures observed in previous simulation were due to single-sized particles which have the same resonant semi-major axis. Here, due to the spread in particle size, the arcs are spread over a few AU and are not visible. This new model gives steady states which can be compared to physical observations of disks.

Now, we can confirm that, in spite of the collisional destruction process, a planet can effectively create asymmetry of about 10 or 20% in the dust disk of β Pictoris. The mean motion resonances can create density structures providing that the normal optical depth and the particle initial eccentricities are not too large ($\tau_{op} \leq \tau_{op_c}$ which is equivalent to $t_{res} \leq 25t_{coll}$, and $e < 0.05$). If observed, these structures could be an indicator of the presence of a massive body.

However, in agreement with Artymowicz (1995), this model is unable to explain neither the very large asymmetry (a factor larger than 3) observed by Lagage and Pantin (1994), nor the asymmetry observed at larger distances until 400 AU (Kallas and Jewitt 1995). Moreover, the maximum optical depth allowed for these asymmetries is also too small to explain the β Pictoris light variations observed on the long time scale (Lecavelier des Etangs *et al.* 1995). Some other new hypothesis now seems to be necessary to explain the phenomena observed in the disk.

ACKNOWLEDGMENTS

REFERENCES

ARTYMOWICZ, P. 1988. Radiation pressure forces on particles in the Beta Pictoris system. *Astrophys. J.* **335,** L79–L82.

ARTYMOWICZ, P. 1995. Modeling and understanding the dust around Beta Pictoris. In *Circumstellar Dust Disk and Planet Formation* (*10th IAP meeting*) (R. Ferlet and A. Vidal-Madjar, Eds.), pp. 47–65. Editions Frontieres.

ARTYMOWICZ, P., C. BURROWS, AND F. PARESCE 1989. The structure of the Beta Pictoris circumstellar disk from combined *IRAS* and coronographic observations. *Astrophys. J.* **337,** 494–513.

BACKMAN, D. E., F. C. GILLETT, AND F. C. WITTERBORN 1992. Infrared observations and thermal model of the β Pictoris disk. *Astrophys. J.* **385,** 670–679.

BACKMAN, D. E., AND F. PARESCE 1993. Main sequence stars with circumstellar solid material: The Vega phenomenon. In *Protostars and Planets III* (E. H. Levy, J. I. Lunine, and M. S. Matthews, Eds.), pp. 1253–1304. Univ. Arizona Press, Tucson.

Burns, J., P. Lamy, and S. Soter 1979. Radiation forces on small particles in the solar system. *Icarus* **40,** 1–48.

Golimowski, D. A., S. T. Durrance, and M. Clampin 1993. Coronographic imaging of the β Pictoris circumstellar disk: Evidence of changing disk structure within 100 AU. *Astrophys. J.* **411,** L41–L44.

Greenberg and Nolan 1989. Delivery of asteroids and meteorites to the inner Solar System. In *Asteroid II* (R. P. Binzel, T. Gehrels, and M. S. Matthews, Eds.), pp. 778–804. Univ. Arizona Press, Tucson.

Kallas, P., and D. Jewitt 1995. Asymmetries in the Beta Pictoris disk. In *Circumstellar Dusk Disk and Planet Formation* (*10th IAP meeting*) (R. Ferlet and A. Vidal-Madjar, Eds.), pp. 371–372. Editions Frontieres.

Lagage, P. O., and E. Pantin 1994. Dust depletion in the inner disk of β Pictoris as a possible indicator of planets. *Nature* **369,** 628–630.

Lazzaro, D., B. Sicardy, F. Roques, and R. Greenberg 1994. Is there a planet around β Pictoris? Perturbations of a planet on a circumstellar dust disk. 2. The analytical model. *Icarus* **108,** 59–80.

Lecavelier des Etangs, A., G. Perrin, R. Ferlet, A. Vidal-Madjar, F. Colas, C. Buil, F. Sèvre, J.-E. Arlot, H. Beust, A. M. Lagrange-Henri, J. Lecacheux, M. Deleuil, and C. Gry 1993. Observations of the central part of the β Pictoris disk with an anti-blooming CCD. *Astron. Astrophys.* **274,** 877–882.

Lecavelier des Etangs, A., M. Deleuil, A. Vidal-Madjar, R. Ferlet, C. Nitschelm, B. Nicolet, and A. M. Lagrange-Henri 1995. β Pictoris: Evidence of light variations. *Astron. Astrophys.* **299,** 557–562.

Le Sergeant d'Hendecourt, L. B., and P. L. Lamy 1980. On the size distribution and physical properties of interplanetary dust grains. *Icarus* **43,** 350–372.

Lein, D. J. 1990. Dust in comets. I. Thermal properties of homogeneous and heterogeneous grains. *Astrophys. J.* **355,** 680–692.

Lissauer, J. J., and C. A. Griffith 1989. Erosion of circumstellar particle disks by interstellar dust. *Astrophys. J.* **340,** 468–471.

Roques, F., H. Scholl, B. Sicardy, and B. A. Smith 1994. Is there a planet around β Pictoris? Perturbations of a planet on a circumstellar dust disk. 1. The numerical model. *Icarus* **108,** 37–58.

Scholl, H., F. Roques, and B. Sicardy 1993. Resonance trapping of circumstellar dust particles by an alleged planet. *Celest. Mech. Dynam. Astron.* **56,** 381–393.

Weidenschilling, S. J., and A. A. Jackson 1993. Orbital resonances and Poynting–Robertson drag. *Icarus* **104,** 244–254.